Supporting Information

For

Is the photochemistry activity weak during haze events?

—— A novel exploration on the photoinduced heterogeneous reaction of NO_2 on mineral dust

Tao Wang[1], Yangyang Liu[1], Yue Deng[1], Hanyun Cheng[1], Yang Yang[1], Yiqing Feng[1], Muhammad Ali Tahir [1], Xiaozhong Fang[1], Xu Dong[1], Kejian Li[1], Saira Ajmal[1], Aziz-Ur-Rahim Bacha[1], Iqra Nabi[1], Hongbo Fu[1], Liwu Zhang[1,2*], Jianmin Chen[1]

[1] Shanghai Key Laboratory of Atmospheric Particle Pollution and Prevention, Department of Environmental Science & Engineering, Fudan University, Shanghai, 200433, Peoples' Republic of China

[2] Shanghai Institute of Pollution Control and Ecological Security, Shanghai, 200092, Peoples' Republic of China

Number of Figures: 14

Number of Tables: 6

Number of Equations: 2

Number of Reactions: 14

Catalogue

Section S1. Particle characterization

Commercial TiO_2 powders (Degussa P25) were employed in this work. Based on the X-ray diffraction (XRD, S4Explorer, Bruker, Germany) analysis, the sample approximately comprises 25% rutile and 75% anatase **(Figure S1a)**. Since the uptake capacity is influenced by particle size **(Zhang et al., 2016)**, prepared particles were passed through a 200-mesh sieve before experiments to make the size uniform.

Transmission electron microscopy (TEM, Nova NanoSem 450, FEI, Japan) image shows the morphology of TiO_2 particles with an average particle size of 12.05±3.46 nm **(Figure S1b, c)**. Additionally, the Brunauer-Emmett-Teller (BET) specific surface area (S_{BET}) of the TiO_2 is measured to be 55.83±0.35 $m^2 \cdot g^{-1}$ (TriStarII3020, Micromeritics Instrument Co., USA).

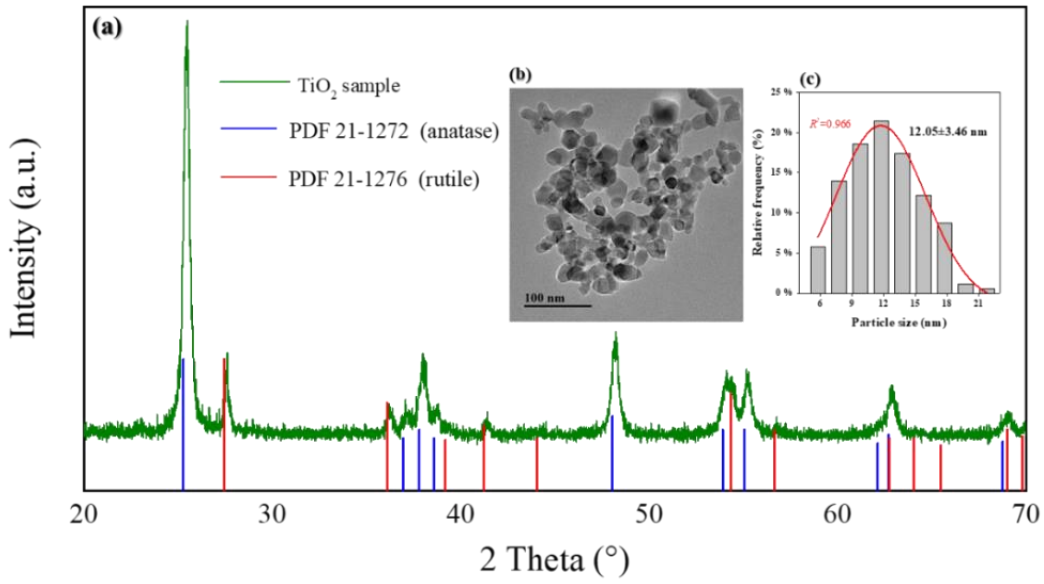

Figure S1. **(a)** XRD pattern for the prepared TiO_2 particles. **(b)** Transmission electron microscopy (TEM) image and **(c)** particle size distribution of TiO_2 nanoparticles. 175 particles were counted to calculate the average size. The distribution is well fitted by a Gaussian function with R^2 of 0.966.

Table S1. Chemical composition of the Kaolin particles.

Components	Proportion (%)
SiO_2	56.93
Al_2O_3	37.49
TiO_2	3.43
Fe_2O_3	1.81
FeO	0.15
K_2O	0.06
P_2O_5	0.05
MgO	0.03
CaO	0.01

Section S2. Experimental setup

In-situ diffuse reflectance infrared Fourier transform spectroscopy (DRIFTS) is helpful in discussing the species formed on particles. The schematic diagram of the in-situ setup is present in **Figure S2**. TiO_2 particles were placed in a ceramic sample cup (0.35 mm depth, 5 mm i.d.). Mass flow controllers (Beijing Sevenstar electronics Co., LTD) were used to adjust the fluxes of reactant gases to the desired flow rate, concentration and relative humidity (RH). A temperature controller was connected to the DRIFTS chamber (Praying Mantis Kit, Harrick) to control the reaction temperature (298 K).

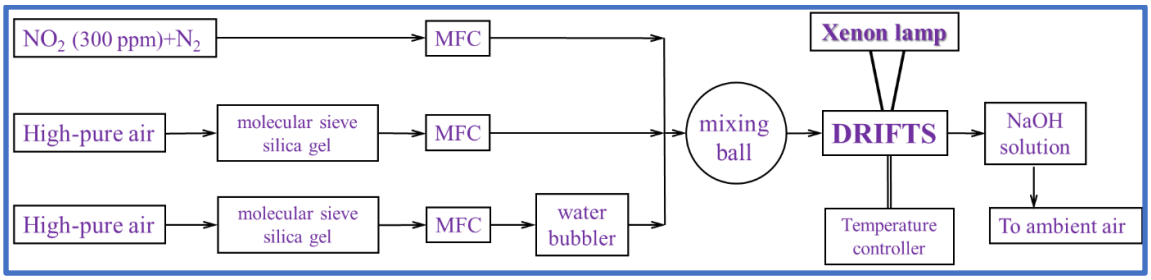

Figure S2. Schematic diagram of experimental setup. The DRIFTS chamber is linked with other parts through Teflon tube. MFC: mass flow controller

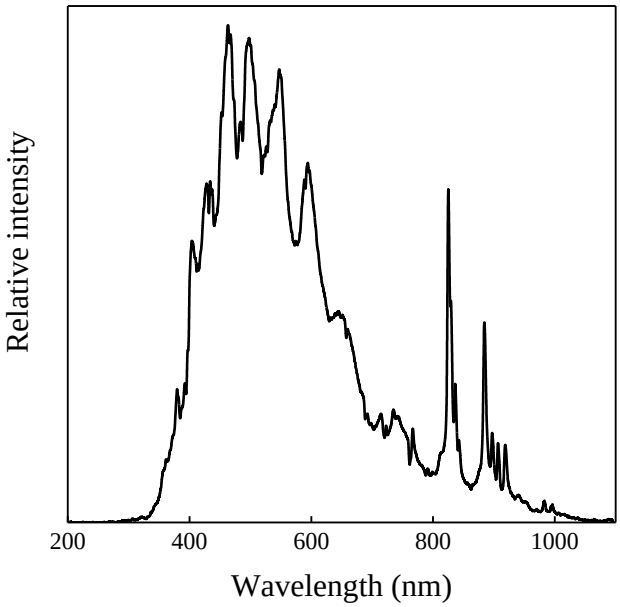

Figure S3. Spectral distribution of the Xenon lamp light measured by a fiber optic spectrometer (AULTT-P4000, Beijing Ceaulight Co., LTD, China).

Section S3. Pretreatment for *in-suit* DRIFTS test

Before the introduction of H_2O into the DRIFTS chamber, the TiO_2 sample was pretreated in a stream of high-pure air (200 ml·min^{-1}) for 60 min to remove the adsorbed water and impurities from the surfaces. A background was recorded before the pretreatment, and then a series of spectra were collected every five minutes.

Negative peaks located at 3700 and 1640 cm^{-1}, as well as the broad bands between 3580-2950 cm^{-1} and centered at 2182 cm^{-1} are attributed to the vibrations of O-H groups. In detail, the peaks at 1640 and 2182 cm^{-1} are assigned to liquid water **(Al-Abadleh and Grassian, 2003; Ma et al., 2010; Zhao et al., 2017)**, whereas the others are characteristics of diverse surface hydroxyl groups **(Deiana et al., 2010; Kong et al., 2014; Nanayakkara et al., 2014)**. Carbonate species formed during sample preparations significantly decreased, as evident by the successive bands around 1500 cm^{-1} **(Chen et al., 2007; Mino et al., 2014)**. All the peaks declined over time and then gradually became stable after 30 min. The spectra of all the mixtures are roughly the same. Therefore, 60 min pretreatment was employed in each experiment.

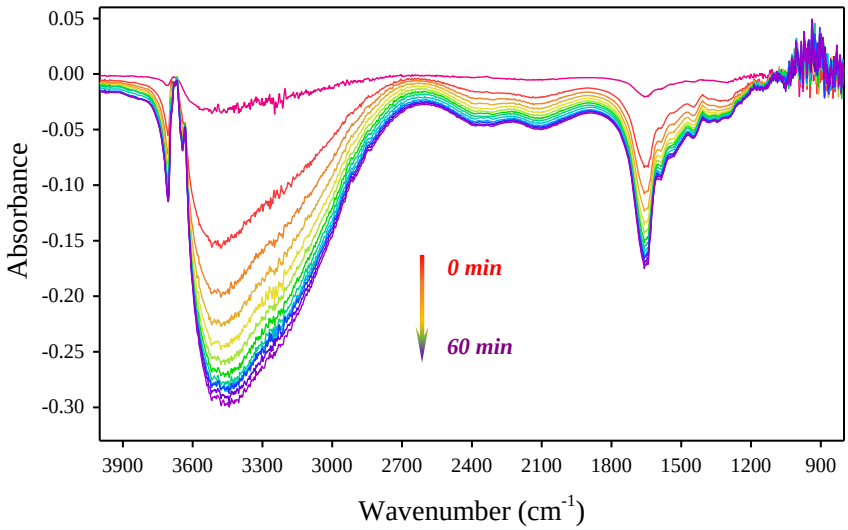

Figure S4. DRIFTS spectra of TiO_2 particles during pretreatment process.

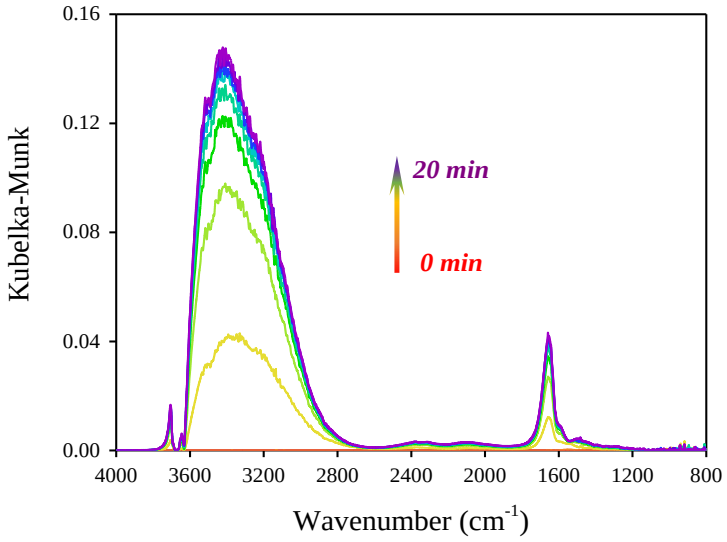

Figure S5. Moisture absorption on TiO_2 particles before NO_2 introduction.

Section S4. *Ex-situ* flow reactor

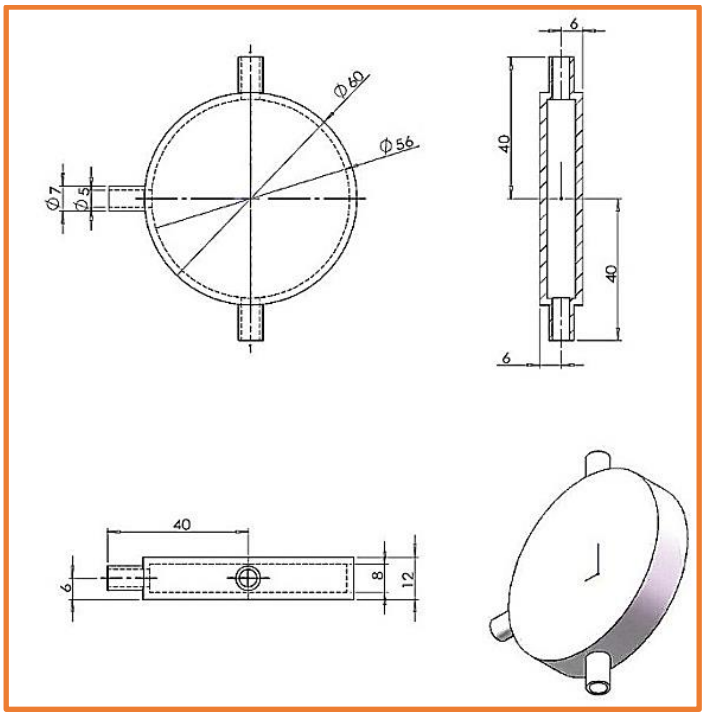

Figure S6. Reactor for the ex-situ experiments.

Section S5. Uptake coefficient estimation

In the estimation of the uptake coefficients, both BET surface area (A_{BET}) and geometric surface area (A_{geo}) are adopted as the reactive surface area (A_s). If the reaction probability is high, the reactants would have no time to diffuse into the sample and the A_s thus be the geometric surface area of the sample cup (A_{geo}). On the contrary, A_{BET}, calculated based on S_{BET} and particle mass (A_{BET}= S_{BET}×mass), would more appropriately represent A_s when the reaction probability is low and the reactants may have enough time to diffuse into the entire sample. Hence, γ-values estimated via A_{BET} and A_{geo} (denoted as γ_{BET} and γ_{geo}, respectively) are mentioned simultaneously to represent the lower and upper limits of γ-values varying with reaction probabilities between the reactants and particles.

Table S2. Parameters for uptake coefficient estimations.

Parameter (unit)		Value
Sulfate formation rate: $d[NO_3^{2-}]/dt$ (ion·s^{-1})		According to reactions
Particle reactive surface area: As (m^2)	A_{BET} (m^2)	S_{BET} × sample mass
	A_{geo} (m^2)	$1.86\times10^{-5}\pm2.16\times10^{-7}$ (*in-situ* DRIFTS reactor) $2.47\times10^{-3}\pm2.46\times10^{-4}$ (*ex-situ* flow reactor)
Reactant concentration: [NO_2] (molecule·m^{-3})		3.773×10^{20} (*in-situ* DRIFTS reaction) 2.215×10^{19} (*ex-situ* flow reaction)
Velocity of molecule: v_{NO_2}	Gas constant: R (J·mol^{-1}·K^{-1})	8.314
	Temperature: T (Kelvin)	298
	Molar mass: M_{NO_2} (kg·mol^{-1})	4.6×10^{-2}
	Pi: π (dimensionless)	3.1416

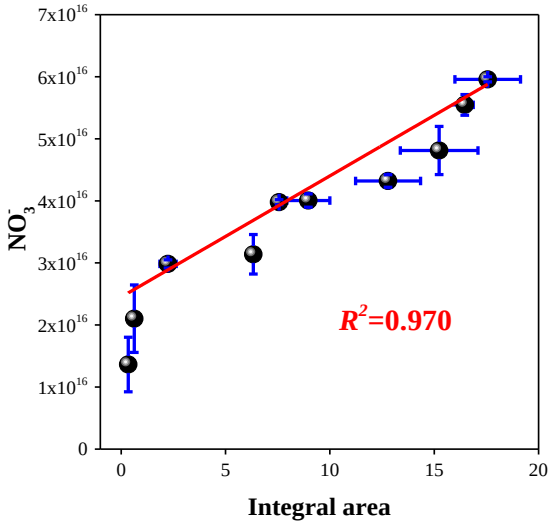

Figure S7. Calibration plot with amount of NO_3^- versus corresponding integrated areas for nitrate.

Table S3. Percentile γ-values (γ_{BET} and γ_{geo}) for the heterogeneous uptake of NO_2 on particles under various light intensities.

Light intensity	γ_{BET}						γ_{geo}					
($mW \cdot cm^{-2}$)	10th	25th	50th	75th	90th	Mean±SD	10th	25th	50th	75th	90th	Mean±SD
0.0	3.93E-12	4.55E-12	5.25E-12	5.97E-12	6.66E-12	5.28E-12±1.07E-12	1.56E-07	1.80E-07	2.07E-07	2.37E-07	2.62E-07	2.08E-07±4.15E-08
0.3	7.92E-12	8.81E-12	9.82E-12	1.09E-11	1.20E-11	9.90E-12±1.56E-12	3.15E-07	3.48E-07	3.89E-07	4.31E-07	4.72E-07	3.90E-07±6.11E-08
5.4	2.56E-11	2.99E-11	3.46E-11	3.98E-11	4.45E-11	3.48E-11±7.28E-12	1.01E-06	1.18E-06	1.37E-06	1.57E-06	1.74E-06	1.37E-06±2.85E-07
17.5	9.17E-11	9.73E-11	1.03E-10	1.10E-10	1.16E-10	1.04E-10±9.51E-12	3.65E-06	3.86E-06	4.09E-06	4.32E-06	4.55E-06	4.11E-06±3.52E-07
23.8	1.07E-10	1.14E-10	1.21E-10	1.28E-10	1.35E-10	1.21E-10±1.08E-11	4.28E-06	4.51E-06	4.77E-06	5.05E-06	5.29E-06	4.78E-06±3.97E-07
30.5	1.19E-10	1.31E-10	1.44E-10	1.58E-10	1.71E-10	1.45E-10±2.03E-11	4.73E-06	5.18E-06	5.70E-06	6.25E-06	6.71E-06	5.75E-06±7.66E-07
54.5	1.67E-10	1.84E-10	2.04E-10	2.25E-10	2.44E-10	2.05E-10±3.08E-11	6.60E-06	7.29E-06	8.06E-06	8.85E-06	9.57E-06	8.10E-06±1.18E-06
98.5	2.04E-10	2.23E-10	2.46E-10	2.69E-10	2.92E-10	2.48E-10±3.47E-11	8.07E-06	8.83E-06	9.71E-06	1.06E-05	1.14E-05	9.77E-06±1.32E-06
128.1	2.37E-10	2.51E-10	2.67E-10	2.83E10	2.98E-10	2.67E-10±2.39E-11	9.42E-06	9.96E-06	1.06E-05	1.11E-05	1.17E-05	1.06E-05±8.88E-07
160.0	2.40E-10	2.61E-10	2.83E-10	3.09E-10	3.32E-10	2.86E-10±3.63E-11	9.51E-06	1.03E-05	1.12E-05	1.22E-05	1.30E-05	1.13E-05±1.39E-06

Table S4. Percentile γ-values (γ_{BET} and γ_{geo}) for the heterogeneous uptake of NO_2 on Kaolin particles under various light intensities.

Light intensity ($mW \cdot cm^{-2}$)		10th	25th	50th	75th	90th	Mean±SD
γ_{BET}	0	6.21E-12	6.99E-12	7.78E-12	8.62E-12	9.38E-12	7.78E-12±1.25E-12
	10	3.56E-10	3.93E-10	4.38E-10	4.81E-10	5.18E-10	4.38E-10±6.14E-11
	40	8.65E-10	8.90E-10	9.17E-10	9.45E-10	9.72E-10	9.18E-10±4.09E-11
	70	9.96E-10	1.06E-09	1.13E-09	1.20E-09	1.27E-09	1.14E-09±1.04E-10
	100	1.01E-09	1.10E-09	1.20E-09	1.30E-09	1.39E-09	1.20E-09±1.46E-10
γ_{geo}	0	2.76E-09	3.12E-09	3.54E-09	4.02E-09	4.47E-09	3.56E-09±6.88E-10
	10	1.58E-07	1.77E-07	2E-07	2.24E-07	2.48E-07	2.01E-07±3.50E-08
	40	3.67E-07	3.9E-07	4.19E-07	4.5E-07	4.84E-07	4.21E-07±4.72E-08
	70	4.38E-07	4.73E-07	5.18E-07	5.66E-07	6.18E-07	5.22E-07±7.08E-08
	100	4.46E-07	4.93E-07	5.46E-07	6.08E-07	6.68E-07	5.51E-07±8.92E-08

In this study, nitrate formation rate under certain light intensity is related to NO_2 concentration, number of active sites on particle surfaces, and O_2 concentration, which is shown by **equation S1** based on the law of mass action.

$$\frac{d[NO_3^-]}{dt} = k[NO_2]^m[Particle]^n[O_2]^p \qquad Eq.S1$$

Where $[NO_3^-]$ is the concentration of products, $[NO_2]$ is the concentration of NO_2, $[Particle]$ is the amount of active sites on particle surfaces, $[O_2]$ is the concentration of O_2, m, n, p are the reaction orders of NO_2, active site and O_2, respectively. Oxygen is sufficient for the oxidation processes. No saturation effects on the formation of nitrate products were observed, and thus the $[Particle]$ is approximately constant. Hence, the product formation rate is largely relative to NO_2 concentration. As reported previously, the reaction order here is determined by double-logarithmic plots of the formation rates versus the NO_2 concentrations based on **equation S2 (Kong et al., 2014; Li et al., 2010; Shang et al., 2010)**.

$$ln(d[NO_3^-]/dt) = mln[NO_2] + nln[Particle] + pln[O_2] + lnk \qquad Eq.S2$$

The reaction orders are 0.90, 0.91, and 1.26 under 14.1, 73.8, and 160 mW/cm^2, respectively, indicating the reaction order of 1 for NO_2 concentration. Therefore, the photoinduced heterogeneous uptake of NO_2 on TiO_2 particles can be viewed as pseudo-first-order reaction.

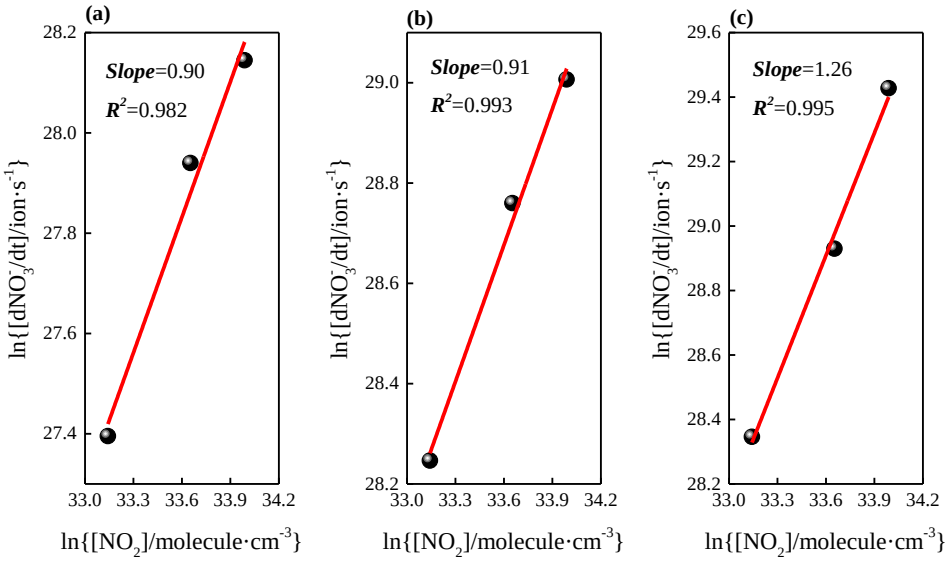

Figure S8. Bilogrithmic plots of the product formation rates versus corresponding NO_2 concentrations under (a) 14.1, (b) 73.8, and (c) 160 mW/cm^2.

Section S6. Field observations

The sampling was performed on the rooftop (~20 m above the ground level to avoid airflow obstruction) of a teaching building (31°20'N, 121°30'E) in Fudan Campus (Shanghai, China) in the late summer and early autumn of 2018 **(Figure S8)**. The sampling site is located in one of the new urban districts of Shanghai, China. Around the sampling site are teaching buildings, residential buildings, and vegetation. A traffic artery is located about 100 m east to the site. The weather situation during sampling was mostly sunny or cloudy, without significant precipitation. Additionally, size distributions of nitrate and nitrite ions collected during diverse periods are summarized in **Figure S9**.

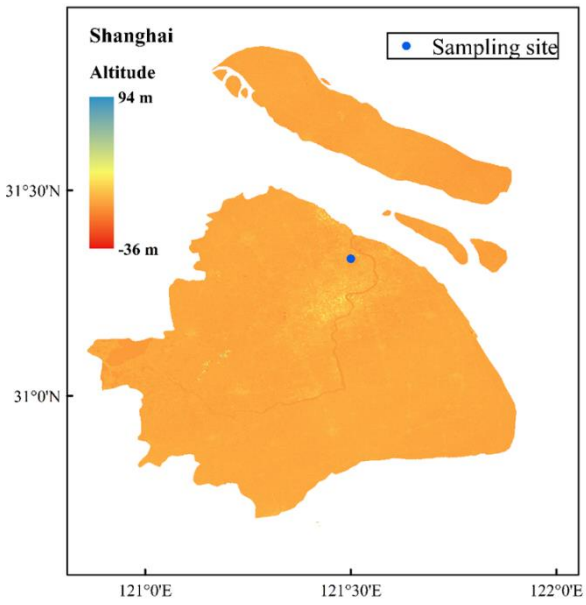

Figure S9. Location of the sampling site in Fudan Campus, Shanghai, China.

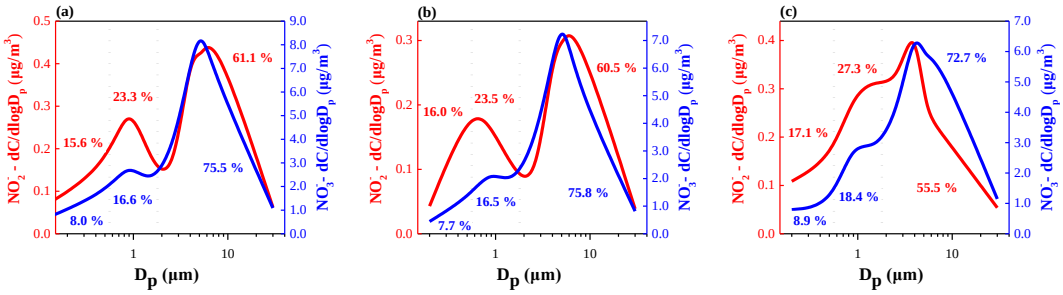

Figure S10. Lognormal size distribution of nitrate and nitrite ions in atmospheric particulates collected during (a) nighttime, (b) daytime, and (c) whole day. The mass fractions of nitrate (blue) and nitrite (red) have been calculated for diverse particle modes.

Section S7. Product observations

As summarized in **Table S3**, the DRIFTS spectra recorded under different conditions are rich in various characteristic peaks, which indicate various surface products.

In order to carefully discuss the reaction pathways, we calculated the proportions of various nitrate/nitrite products under different conditions **(Figure 10)**.

Table S5. Main absorption bands observed on TiO_2 particles.

Wavenumber/cm^{-1}	Species
1195, 1440	Monodentate nitrite
1308	Bidentate nitrite
1312, 1553	Monodentate nitrate
1276, 1573	Bidentate nitrate
1602	Bridging nitrate
1347, 1412	Water-solvated nitrate

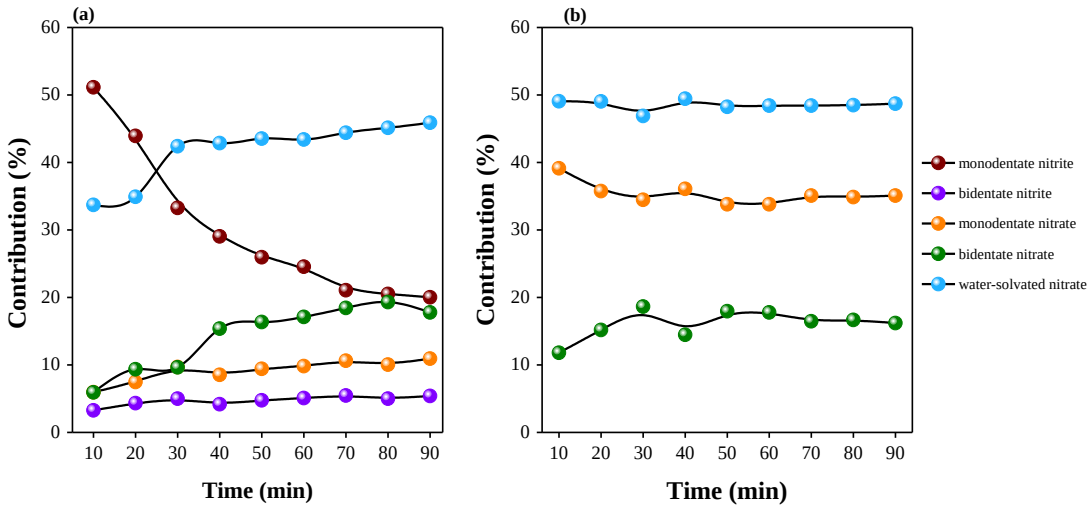

Figure S11. Contributions of diverse nitrogen compounds to the total products as a function of reaction time under (a) dark condition and (b) illumination (I=98.5 mW/cm^2).

Section S8. Detailed reactions in photocatalytic process

Apart from the reactions referred in the manuscript ***(R.1-7)***, some additional reactions are listed below according to some previous studies **(Park et al., 2017; Shang et al., 2017)**.

$$NO_{2(g)} \leftrightharpoons NO_{2(ads)} \qquad R.(S1)$$

$$2NO_{2(ads)} + 2M - OH \rightarrow M - NO^{-}_{3(ads)} + M - NO^{-}_{2(ads)} + H_2O \qquad R.(S2)$$

$$2NO_{2(ads)} + H_2O \rightarrow HNO_3 + HNO_2 \qquad R.(S3)$$

$$HNO_3 \leftrightharpoons NO^{-}_{3(free)} + H^+ \qquad R.(S4)$$

$$HNO_2 \leftrightharpoons NO^{-}_{2(free)} + H^+ \qquad R.(S5)$$

$$T_iO_2 + hv(\lambda \leq 390nm) \rightarrow h^+ + e^- \qquad R.(S6)$$

$$h^+ + H_2O \rightarrow {}^{\cdot}OH + H^+ \qquad R.(S7)$$

$$e^- + O_2 \rightarrow O_2^{\cdot -} \qquad R.(S8)$$

$$e^- + O_2 + H^+ \rightarrow HO_2^{\cdot} \qquad R.(S9)$$

$$2h^+ + 2H_2O \rightarrow H_2O_2 + 2H^+ \qquad R.(S10)$$

$$2O_2^{\cdot -} + 2H^+ \rightarrow H_2O_2 + O_2 \qquad R.(S11)$$

$$HO_2^{\cdot} + NO \rightarrow NO_2 + {}^{\cdot}OH \qquad R.(S12)$$

$$H_2O_2 + hv \rightarrow 2\,{}^{\cdot}OH \qquad R.(S13)$$

$$HONO + hv \rightarrow NO + {}^{\cdot}OH \qquad R.(S14)$$

Section S9. Photoinduced nitrite oxidation

'TiO_2-nitrite' mixture was prepared with a 10 % mass fraction of $NaNO_2$. The mixture was then used as model particles for DRIFTS test under dark condition and illumination (98.5 mW/cm^2) in a flow of 100 ml/min high-pure air (RH≈40%) for 60 min. Nitrate products are easily observed after illumination reaction, while was not apparent after dark process, highlighting the photocatalytic oxidation of nitrite intermediates to nitrate products. Hence, nitrate products on particles may stem from nitrite oxidation by photoinduced active species **(R.5)** besides the oxidation by NO_2 and other nitrite species **(R.3, 4)**.

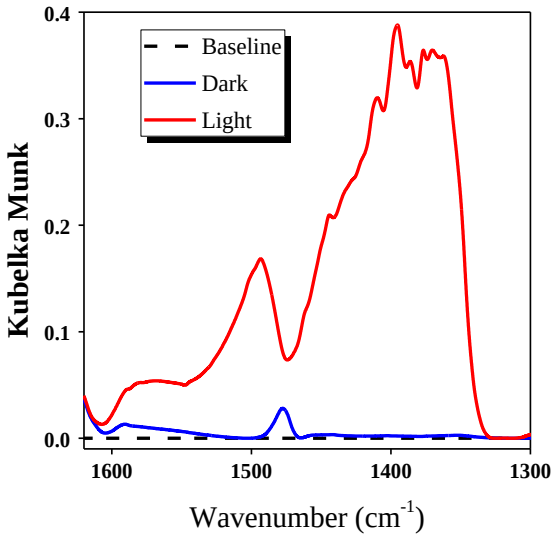

Figure S12. DRIFTS spectra for nitrate products formed on TiO_2-$NaNO_2$ mixture after 60 min exposure to humid high-pure air (RH≈40%) under dark and light condition (I=98.5 mW/cm^2).

Section S10. Raman detection

The nitrate products were detected by a confocal Raman spectrometer (Jobin Yvon Horiba Gr, France) after dark reaction and illumination reaction (98.5 $mW \cdot cm^{-2}$) in DRIFTS chamber. The Raman scattering was excited by an external-cavity diode (532 nm) and coupled with a 50× microscope objective (Olympus, 0.90 Numerical Aperture). The backscattering signals were acquired by a charge-coupled device (CCD) camera. Each spectrum ranging from 100 to 4000 cm^{-1} was obtained with quartic repeated scans and a total exposure time of 60 s. Thirty point scans were carried out for each sample, and the average results were used to reveal the general situation.

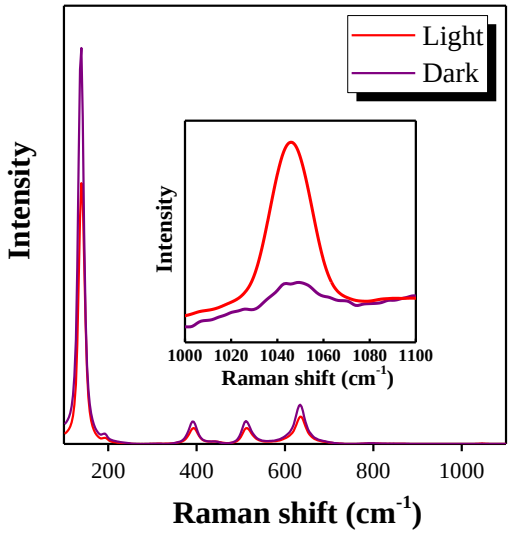

Figure S13. Raman spectra for particles after illumination reaction (I=98.5 Mw/cm^2, red) and dark reaction (purple).

Section S11. Sensitivity analysis

The results of sensitivity analysis is shown in **Figure S9** with slope and *f* contribute most to the total variance of γ_{BET} and γ_{geo}, followed by S_{BET} and m for γ_{BET}, and A_{geo} for γ_{geo}. Detailed contributions are present in **Tables S3**.

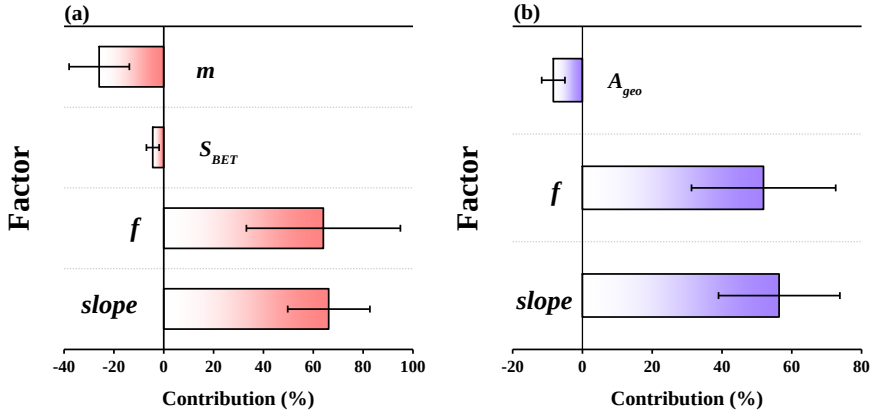

Figure S14. Sensitivity analysis on **(a)** γ_{BET} and **(b)** γ_{geo}.

Table S6. Results of sensitivity analysis.

γ_{BET}		**γ_{geo}**	
Factor	Contribution (%)	Factor	Contribution (%)
m	-28±13	A_{geo}	-7±3
S_{BET}	-5±2	*f*	51±20
f	66±32	slope	56±17
slope	67±16		

References

Al-Abadleh, H.A., Grassian, V.H.: FT-IR Study of Water Adsorption on Aluminum Oxide Surfaces, Langmuir, 19, 341-347, doi: 10.1021/la026208a, 2003.

Chen, H., Kong, L., Chen, J., Zhang, R., Wang, L.: Heterogeneous Uptake of Carbonyl Sulfide on Hematite and Hematite−NaCl Mixtures, Environ. Sci. Technol., 41, 6484-6490, doi: 10.1021/es070717n, 2007.

Deiana, C., Fois, E., Coluccia, S., Martra, G.: Surface Structure of TiO_2 P25 Nanoparticles: Infrared Study of Hydroxy Groups on Coordinative Defect Sites, The Journal of Physical Chemistry C, 114, 21531-21538, doi: 10.1021/jp107671k, 2010.

Kong, L.D., Zhao, X., Sun, Z.Y., Yang, Y.W., Fu, H.B., Zhang, S.C., Cheng, T.T., Yang, X., Wang, L., Chen, J.M.: The effect of nitrate on the heterogeneous uptake of sulfur dioxide on hematite, Atmos. Chem. Phys., 14, 9451-9467, doi: org/10.5194/acp-14-9451-2014, 2014.

Li, J., Shang, J., Zhu, T.: Heterogeneous reactions of SO_2 on ZnO particle surfaces, Science China Chemistry, 54, 161-166, doi: org/10.1007/s11426-010-4167-9, 2010.

Ma, Q., He, H., Liu, Y.: In situ DRIFTS study of hygroscopic behavior of mineral aerosol, J. Environ. Sci.-China, 22, 555-560, doi: org/10.1016/S1001-0742(09)60145-5, 2010.

Mino, L., Spoto, G., Ferrari, A.M.: CO_2 Capture by TiO_2 Anatase Surfaces a Combined DFT and FTIR Study, J. Phys. Chem. C, 118, 25016-25026, doi: 10.1021/jp507443k, 2014.

Nanayakkara, C.E., Larish, W.A., Grassian, V.H.: Titanium Dioxide Nanoparticle Surface Reactivity with Atmospheric Gases, CO_2, SO_2, and NO_2: Roles of Surface Hydroxyl Groups and Adsorbed Water in the Formation and Stability of Adsorbed Products, The Journal of Physical Chemistry C, 118, 23011-23021, doi: 10.1021/jp504402z, 2014.

Park, J., Jang, M., Yu, Z.: Heterogeneous Photo-oxidation of SO_2 in the Presence of Two Different Mineral Dust Particles: Gobi and Arizona Dust, Environ. Sci. Technol., 51, 9605-9613, doi: 10.1021/acs.est.7b00588, 2017.

Shang, J., Li, J., Zhu, T.: Heterogeneous reaction of SO_2 on TiO_2 particles, Science China Chemistry, 53, 2637-2643, doi: org/10.1007/s11426-010-4160-3, 2010.

Shang, J., Xu, W.W., Ye, C., George, C., Zhu, T.: Synergistic effect of nitrate-doped TiO_2 aerosols on the fast photochemical oxidation of formaldehyde, Sci. Rep.-UK, doi: 10.1038/s41598-017-01396-x, 2017.

Zhang, Y., Tong, S.R., Ge, M.F.: A study about the influence of the size of $CaCO_3$ on the heterogeneous oxidation of sulfur dioxide by ozone, Spectrosc. Spect. Anal., 36, 126-127, doi:2016.

Zhao, Y., Liu, Y., Ma, J., Ma, Q., He, H.: Heterogeneous reaction of SO_2 with soot: The roles of relative humidity and surface composition of soot in surface sulfate formation, Atmos. Environ., 152, 465-476, doi: 10.1016/j.atmosenv.2017.01.005, 2017.